Electronic Supplementary Material (ESI) for Journal of Materials Chemistry A.
This journal is © The Royal Society of Chemistry 2019

Supporting Information

Ultrapermeable graphene oxide membranes with tunable interlayer distance *via* vein-like supramolecular dendrimers

Yimeng Song, Run Li, Fusheng Pan, Ze He, Hao Yang, Ying Li, Leixin Yang, Meidi Wang, Hongjian Wang, Zhongyi Jiang**

Preparation of GO dispersion.

The detail about GO dispersion preparation was described in our previous work.[1] Briefly, 115 mL concentrated H_2SO_4 (98 wt%) was cooled under 0°C followed by adding 5 g natural graphite powder and 2.5 g $NaNO_3$ and the mixture was mechanically stirred (500 rpm) under 0°C. Afterward, 15 g $KMnO_4$ was slowly added in batches during a period of at least 20 min. After being stirred for another 2 h, the mixture was heated to 35°C and further stirred for 3 h. 230 mL deionized water was slowly added to the mixture with the temperature maintaining below 90°C. The temperature was then raised to 95°C and remained 30 min. Subsequently, the cooled mixture was slowly poured into 1 L deionized water followed by the addition of 30 mL 30wt% H_2O_2 aqueous solution in order to remove the residual $KMnO_4$ and MnO_2. The mixture was then washed with 5% HCl and with excess water until the pH reached 5, followed by a 9-day dialysis. Finally, a yellow-brown GO aqueous dispersion was obtained by ultrasonicating the above product for 1 h and then centrifuging at 10000 rpm to remove the incompletely exfoliated or large portions.

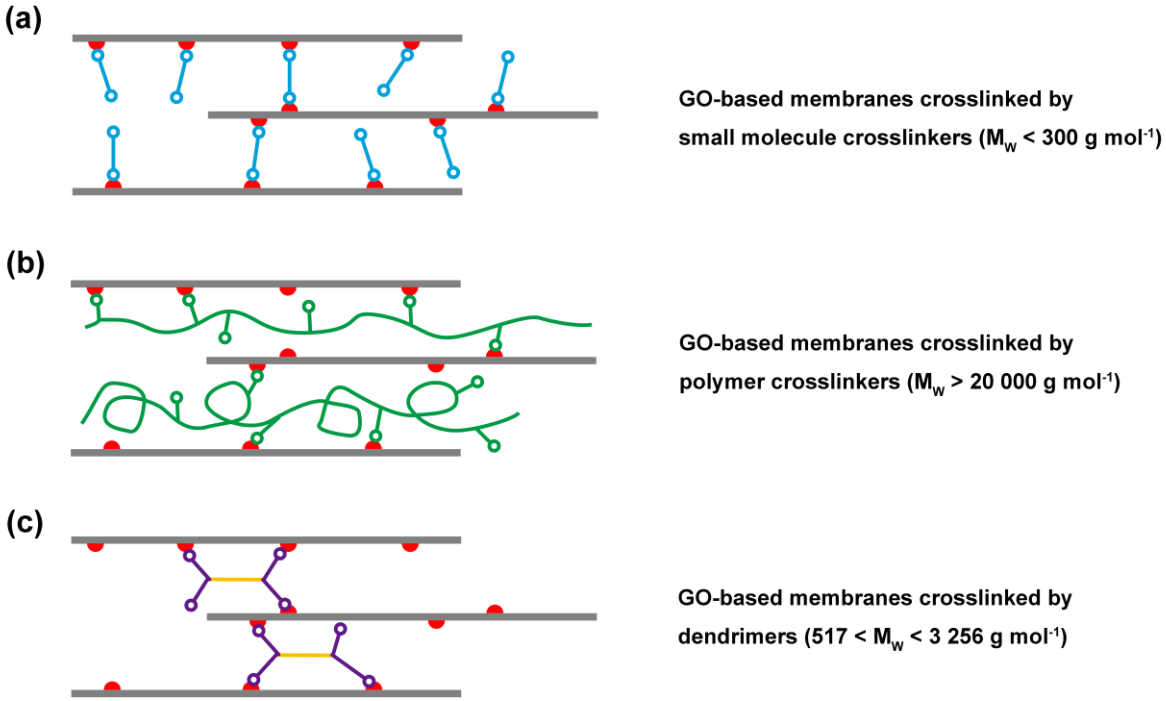

Fig.S1 GO-based membranes crosslinked by different crosslinkers. a) Small molecule crosslinkers. b) Polymer crosslinkers. c) Dendrimers.

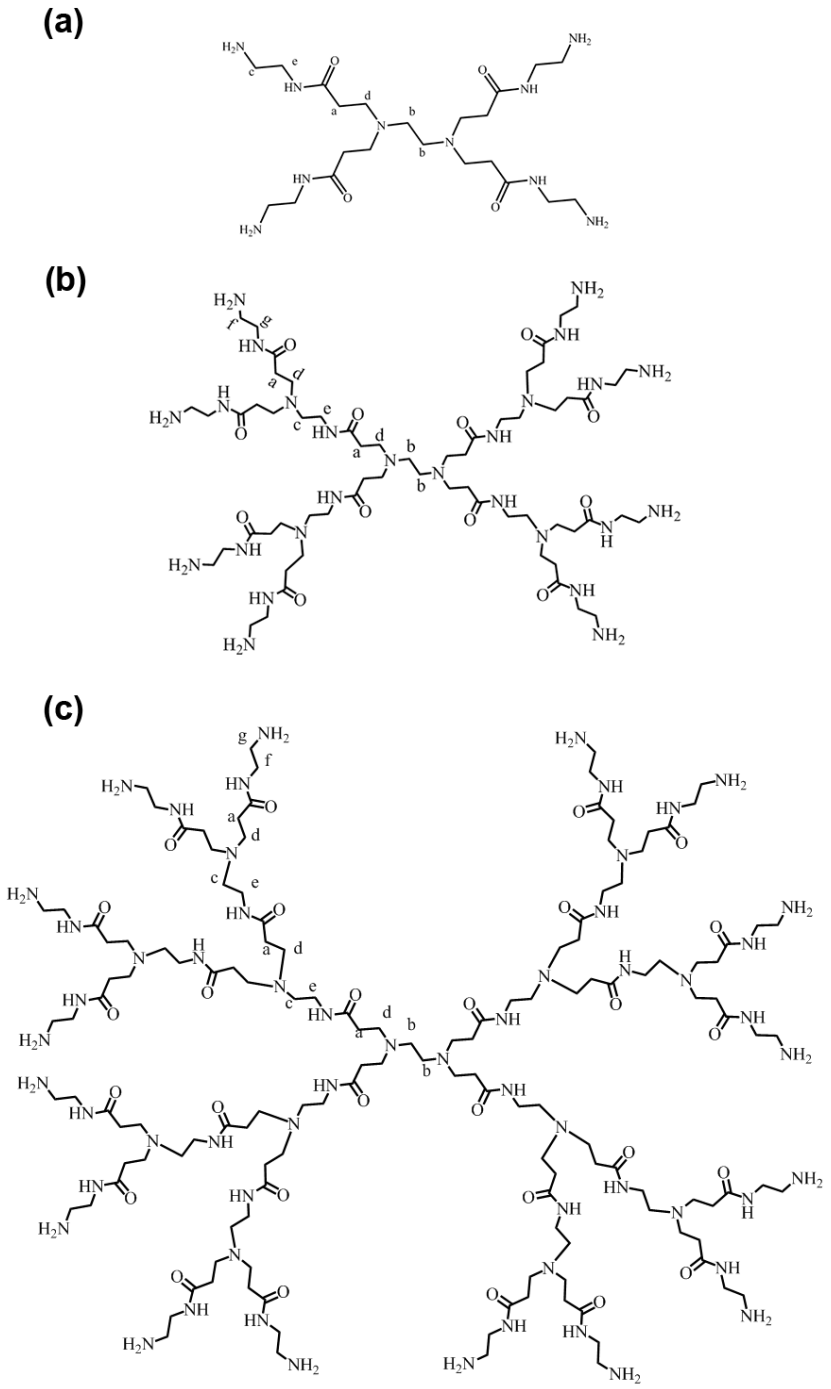

Fig.S2 Structure diagram of PAMAM dendrimers a) Generation 0 (G_0), ^{1}H NMR (400 MHz, D_2O, δ): 3.25 (8H, e), 2.82 (8H, d), 2.73 (8H, c), 2.61 (4H, b), 2.45 (8H; a); b) Generation 1 (G_1), ^{1}H NMR (400 MHz, D_2O, δ): 3.30 (8H, e), 3.24 (8H, g), 2.83 (24H, d), 2.67~2.71 (16H, f), 2.63~2.67 (8H, c), 2.62 (4H, b), 2.43 (24H, a); c) Generation 2 (G_2), ^{1}H NMR (400 MHz, D_2O, δ): 3.30 (24H, e), 3.26 (32H, g), 2.83 (56H, d), 2.74 (32H, f), 2.63 (24H, c), 2.62 (4H, b), 2.43 (56H, a).

Table S1 Properties of PAMAM dendrimers G_0, G_1, G_2.

	G_0	**G_1**	**G_2**
Molecular formula	$C_{22}H_{48}N_{10}O_4$	$C_{62}H_{128}N_{26}O_{12}$	$C_{142}H_{288}N_{58}O_{28}$
Molecular weight [Da]	517	1430	3256
Number of atoms	84	228	516
Terminal nitrogens	4	8	16
Measured radius [nm]	1.5	2.2	2.9
Radius of gyration R_N [a)] [nm]	0.68	1.04	1.16
Diffusion coefficient [b)] [$\times 10^6$ cm^2 s^{-1}]	1.70	1.15	0.88

[a)] Reported by Goddard et al[2]; [b)] The diffusion coefficient is calculated based on Stokes-Einstein equation at 37 ^oC[3].

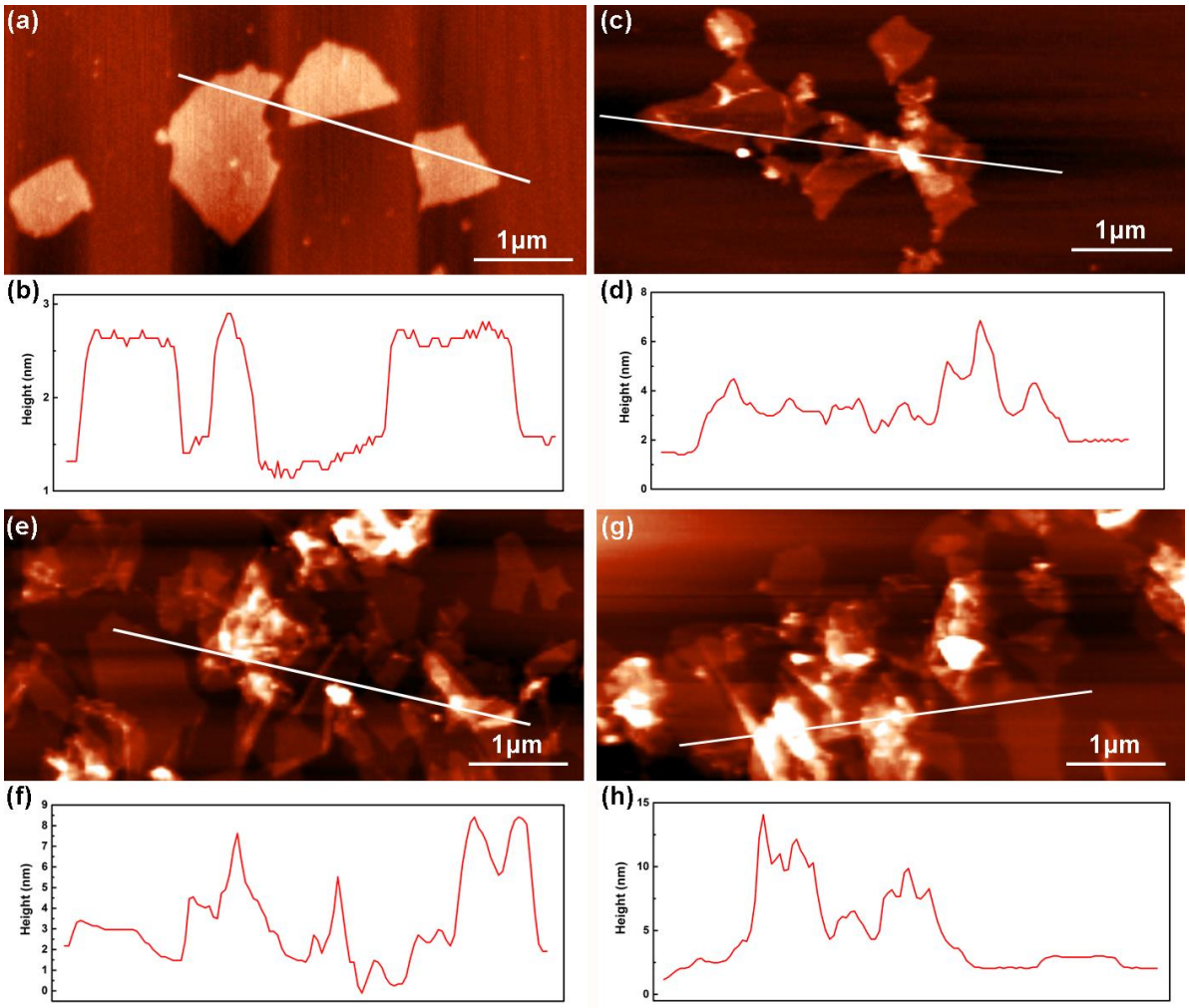

Fig.S3 AFM images and height profiles of a)-b) GO nanosheets and electrostatic assembled c)-d) GO@G_0, e)-f) GO@G_1 and g)-h) GO@G_2. (Scale bars 1 μm)

The reaction approaches of GO with PAMAM.

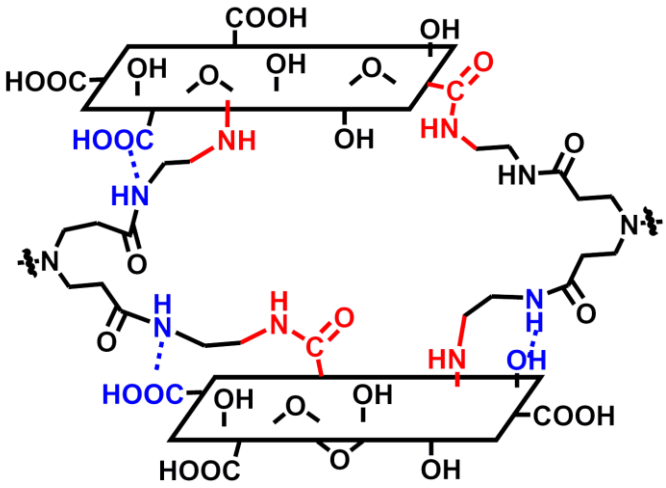

Dehydration condensation:

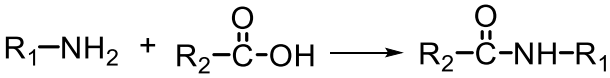

Nucleophilic addition:

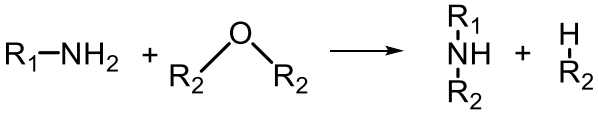

Table S2 XPS elemental analyses of GO, GO-G_0, GO-G_1 and GO-G_2 membranes.

	C [at%] [a)]	O [at%]	N [at%]
GO	67.61	30.32	1.65
GO-G_0	67.70	26.61	2.61
GO-G_1	62.67	28.84	4.85
GO-G_2	63.13	24.24	7.57

Table S3 XPS elemental analyses of GO, GO-G_0, GO-G_1 and GO-G_2 membranes in the C1s region.

	Bond type ratio			
	C-C/C=C	C-O/C-N	C-O-C	C=O
GO	46.04%	7.42%	42.53%	4.01%
GO-G_0	51.40%	10.18%	33.49%	4.94%
GO-G_1	49.25%	12.29%	33.11%	5.35%
GO-G_2	47.82%	17.90%	28.47%	5.82%

Table S4 XPS elemental analyses of GO, GO-G_0, GO-G_1 and GO-G_2 membranes in the N1s region.

	Bond type ratio			
	$-NH_2$	-N-C=O	-NH	$-NO_3$
GO		45.69%		54.31%
GO-G_0	24.52%	34.21%	28.87%	12.39%
GO-G_1	13.76%	41.27%	34.39%	10.58%
GO-G_2	18.93%	41.64%	37.85%	1.59%

Table S5 Kinetic diameter and hydrated diamter of different solvent molecules and ions.[4, 5]

	Kinetic diameter [Å]	Hydrated diameter [Å]
water	2.8	
ethanol	4.3	
i-propanol	4.7	
n-butanol	5.1	
i-butanol	5.1	
Na^+		7.2
Cl^-		6.6

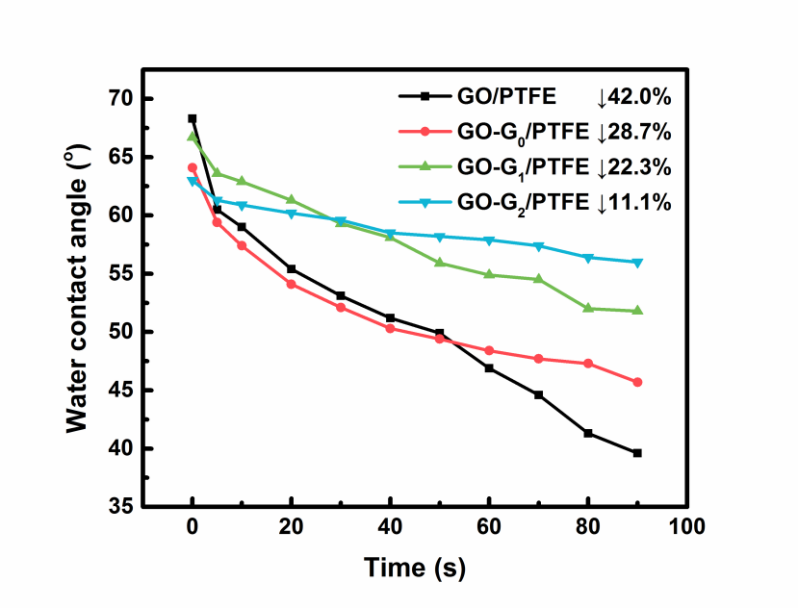

Fig.S4 The water contact angle of GO/PTFE, GO-G_0/PTFE, GO-G_1/PTFE and GO-G_2/PTFE membranes in 90 s at ambient temperature.

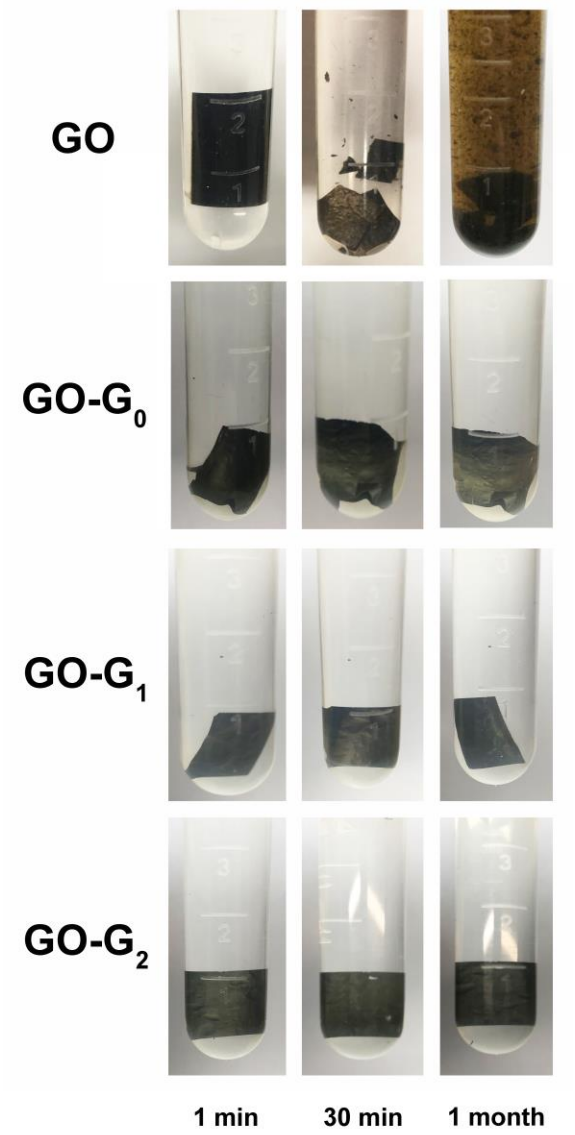

Fig.S5 Stability of GO, GO-G_0, GO-G_1 and GO-G_2 membranes in water for different time periods (1 min, 30 min and 1 month).

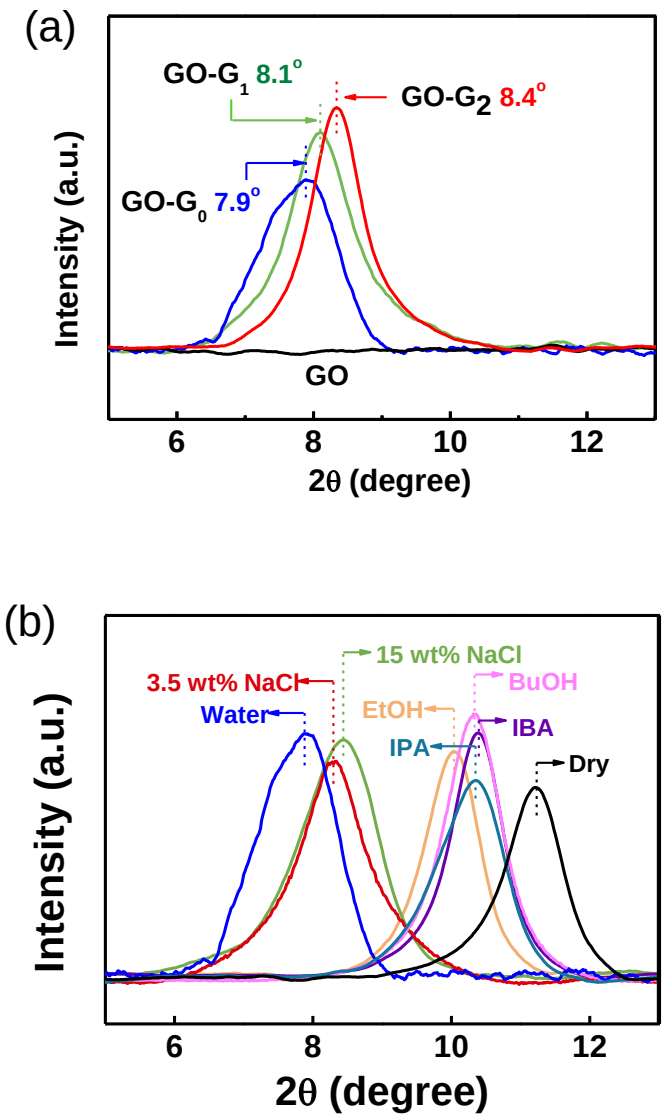

Fig.S6 (a) XRD patterns of GO, GO-G_0, GO-G_1, and GO-G_2 membranes in water. (b) XRD patterns of GO-G_0 membranes under different environments, either totally dried or immersed in different solvents.

Table S6 The interlayer distance of GO-G_0 membranes under different conditions.

	Dry	Water	3.5wt% NaCl	15wt% NaCl	EtOH	IPA	IBA	BuOH
2θ[º]	11.2	7.9	8.3	8.4	10.1	10.3	10.3	10.4
Interlayer distance [nm]	0.44	0.76	0.72	0.71	0.52	0.51	0.51	0.50

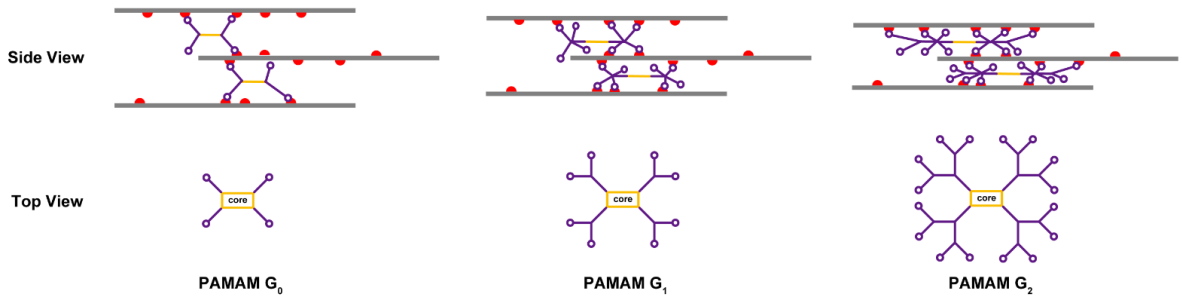

Fig.S7 Schematic of the PAMAM crosslinkers (side view) in the 2D naonchannels and schematic diagram of PAMAM crosslinkers (top view).

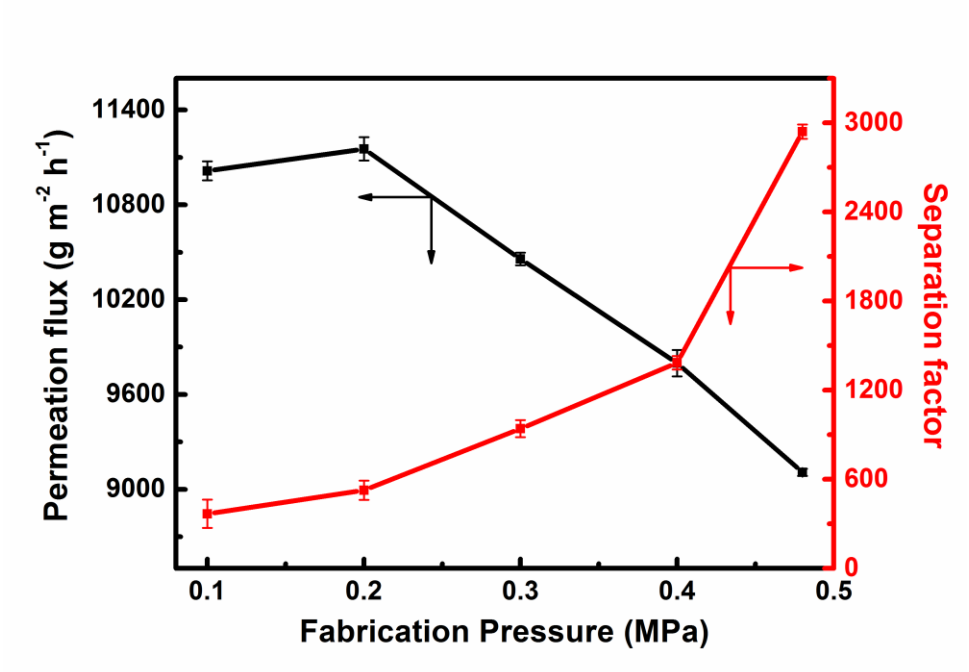

Fig.S8 Separation performance of GO-G_0/PTFE membranes fabricated under different filtration pressure. The thickness of selective layer was ~180 nm. The feed was kept at 80ºC, containing 90 wt% of *n*-butanol and 10 wt% water.

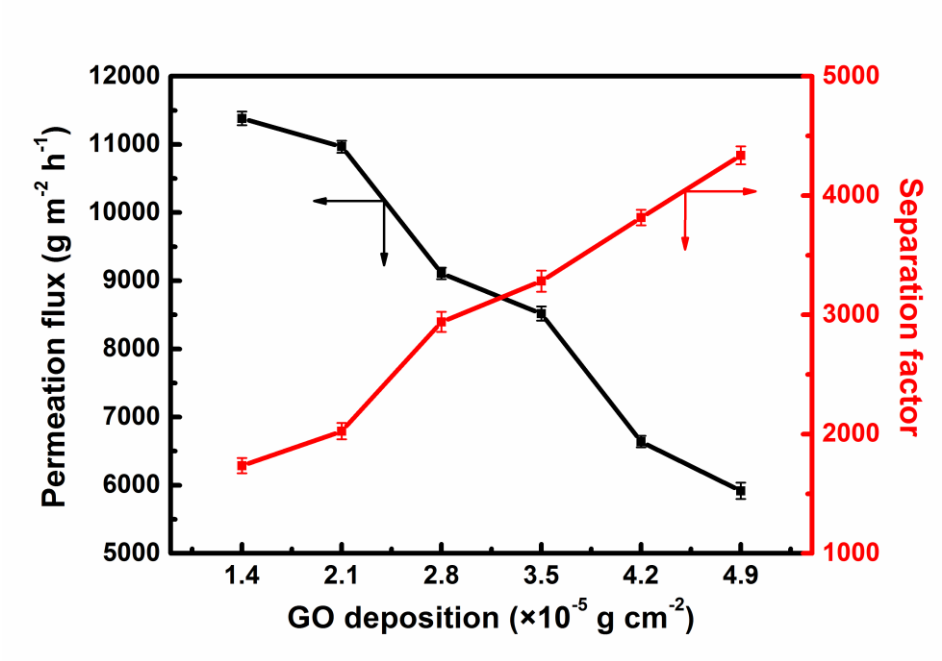

Fig.S9 Separation performance of GO-G_0/PTFE membranes fabricated with different GO deposition. The feed was kept at 80°C, containing 90 wt% of *n*-butanol and 10 wt% water.

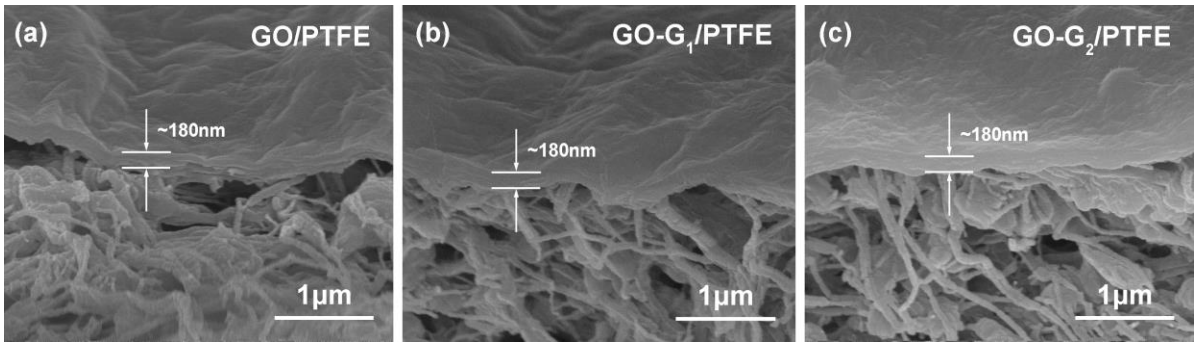

Fig.S10 SEM images of a) GO/PTFE, b) GO-G_1/PTFE, and c) GO-G_2/PTFE.

Table S7 Comparison of the butanol dehydration performance of GO-G_0/PTFE, GO-G_1/PTFE and GO-G_2/PTFE membranes in this study with literature results.

Membrane material	Feed composition [wt%]	Feed temperature [°C]	Flux [g m^{-2} h^{-1}]	Separation factor	Reference
PVA/ceramic hollow fiber	*n*-Butanol/Water (95/5)	80	1000	450	6
6FDA-ODA-NDA/Ultem® 1010	*n*-Butanol/Water (95/5)	60	390	2518	7
Mont-25	*n*-Butanol/Water (95/5)	28	7000	36	8
PVA-CS/ceramic	*i*-Butanol/Water (90/10)	70	1116	1000	9
QP4VP/CMCNa	*n*-Butanol/Water (90/10)	60	2241	1116	10
SA-HEC	*t*-Butanol/Water (87/13)	30	2300	3237	11
NaY zeolite	*n*-Butanol/Water (90/10)	75	4560	1020	12
Zeolite LTA	*i*-Butanol/Water (95/5)	100	4460	3272	13
Methylated silica	*n*-Butanol/Water (94/6)	60	1500	1000	14
Zeolite LTA	*i*-Butanol/Water (95/5)	60	1210	2811	13
Hollow fiber silica	*n*-Butanol/Water (95/5)	80	2920	1200	15
GO/ceramic	*t*-Butanol/Water (90/10)	70	1630	5120	16
GO/ceramic	*s*-Butanol/Water (90/10)	70	1820	6910	16
GO-GTA	*n*-Butanol/Water (85/15)	60	2593	1883	17
CS@GO/hollow fiber	*n*-Butanol/Water (90/10)	70	10124	1523	18
GOPASA/mPAN	*i*-Butanol/Water (90/10)	30	2540	2241	19
GOPASA/mPAN	*i*-Butanol/Water (90/10)	70	4340	1791	19
GO-G_0/PTFE	*n*-Butanol/Water (90/10)	80	9108	2941	This work
GO-G_1/PTFE	*n*-Butanol/Water (90/10)	80	8742	3186	This work
GO-G_2/PTFE	*n*-Butanol/Water (90/10)	80	6096	3688	This work

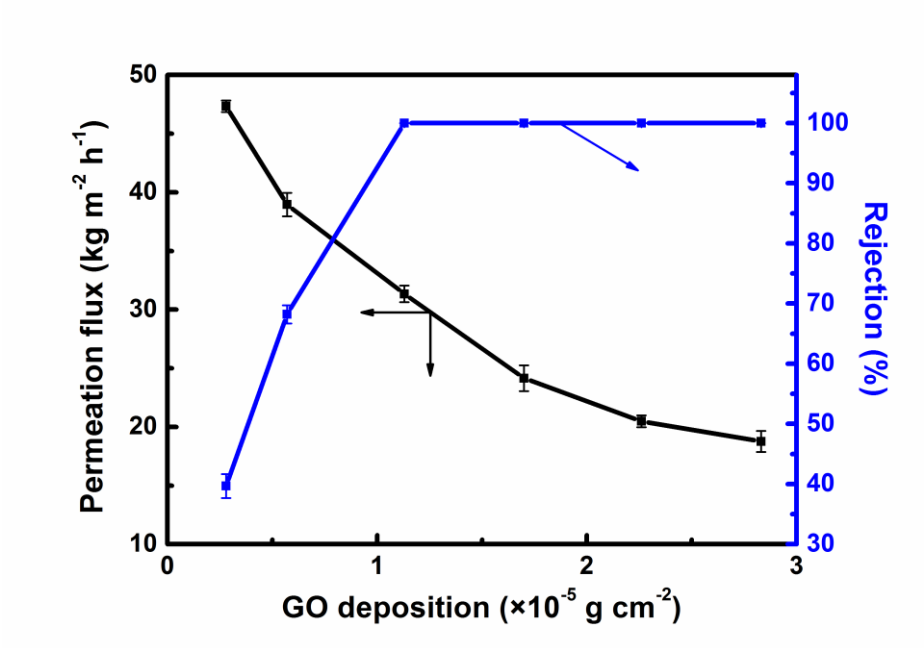

Fig.S11 Desalination performance of GO-G_0/PTFE membranes fabricated with different GO deposition. The feed was 3.5 wt% NaCl solution and kept at 30°C. The cross flow speed is 60 L h^{-1} and the permeate side absolute pressure is 0.1 kPa.

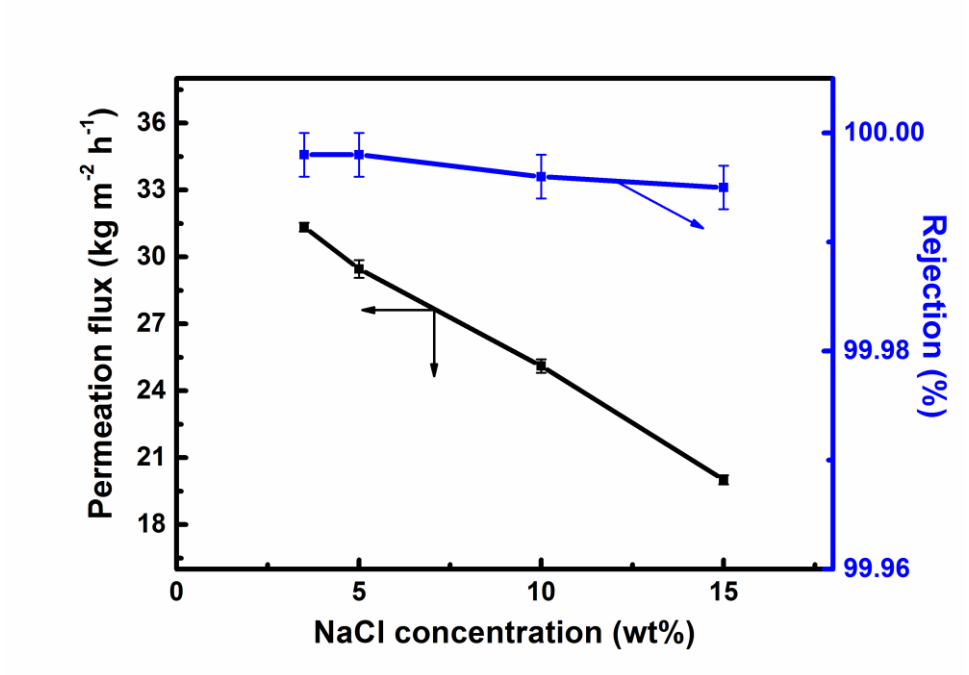

Fig.S12 Desalination performance of GO-G_0/PTFE membranes with different NaCl concentrations in feed at 30°C. The cross flow speed is 60 L h^{-1} and the permeate side absolute pressure is 0.1 kPa. The thickness of selective layer was ~60 nm.

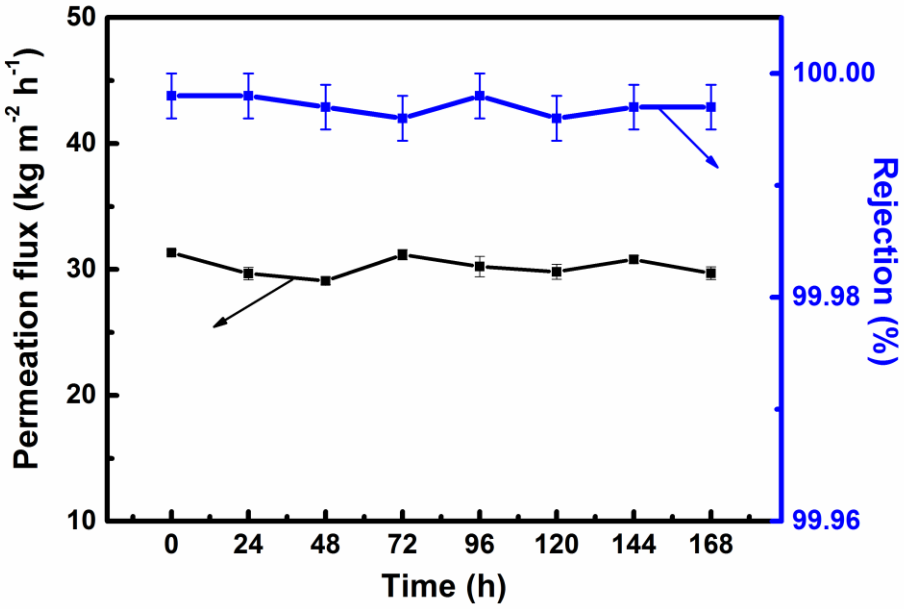

Fig.S13 Long-term desalination performance of GO-G_0/PTFE membranes with 60nm-thick selective layer. The feed was 3.5 wt% NaCl solution and kept at 30°C. The cross flow speed is 60 L h^{-1} and the permeate side absolute pressure is 0.1 kPa.

Table S8 Comparison of the desalination performance of GO-G_0/PTFE membrane in this study with literature results.

Material	Feed NaCl concentration [wt%]	Temperature [°C]	Permeantion flux [kg m^{-2} h^{-1}]	Rejection [%]	Reference
PVA	3.5	25	7.36	99.8	20
Silica/PVA	3.5	22	6.93	99.5	20
NaA zeolite	3.5	69	1.9	99.9	21
GO/ceramic	3.5	90	48.4	99.7	22
GOF/ceramic	3.5	45	3.4	99.9	22
GOF/ceramic	3.5	90	11.4	99.9	22
GO/PAN	3.5	30	14.3	99.8	23
GO/PAN	3.5	90	65.1	99.8	23
GO/PAN	10	30	11.2	99.8	23
MXene/PAN	3.5	30	48.2	99.5	24
MXene/PAN	3.5	65	85.4	99.5	24
MOF/PVA	2	80		>99.999	25
GO/PAN	3.5	70	69.1	99.9	26
GO/PI	3.5	90	15.6	99.8	27
GO/PI	10	75	10.7	99.9	28
Cellulose triacetate	10	50	2.3	99.0	29
Cellulose acetate	4-14	70	5.97-2.45	99.7	30
PVA	0.5	20	9.04	99.5	31
PVA	5	~25	5.57	99.5	31
S-PVA/PAN	3.5	70	46.3	99.5	32
S-PVA/PAN	3.5	30	14.11	99.7	32
MFI-zeolite	3.5	21	4	80	33
S-SEBS 54.1%	1	63	22.87	99.9	34
PVA	3	70	7.4	99.9	35
Silicalite-1	0.3	75	11.5	99	36
ZSM-5	0.3	75	12.5	99	36
PVA/maleic anhydride/silica	0.2	65	11.7	99.9	37
Clinoptilolite-phosphate	0.14	95	15	95	38
CS/GO-1	3.5	60	17.7	99.99	39
CS/GO-1	10	60	16.2	99.99	39
Sulfosuccinic acid cross-linked PVA	10	70	11.2	99.8	40
PVA/maleic anhydride/silica	0.2	22	6.9	99.5	41
PVA/silica	0.2	60	20.4	99.9	42
PVA/silica	3	60	10.4	99.9	42
GO-G_0/PTFE	3.5	30	31.34	>99.99	This work
GO-G_0/PTFE	3.5	70	124.11	>99.99	This work

Predictive model of water flux within GO-based membranes.

The mathematical model was established based on Lan's study[43], modified by characteristic parameters of GO-based membranes. The model was developed under consideration of both mass transfer and heat transfer processes.

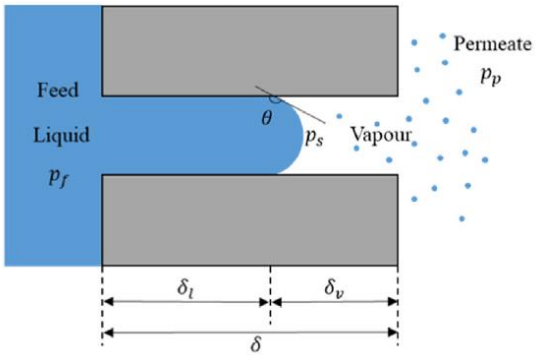

Fig.S14 Schematic of water flow inside the interlayer nanochannel of a GO membrane[43]

The weight flow rate of vapor (kg/s) and liquid (kg/s) inside the 2D nanochannels of GO membranes was governed by the Knudsen flow (S2) and Couette flow (S3)[44]:

$$N_v = \frac{d^2 L}{\delta_v}\left(\frac{32M}{9\pi RT}\right)^{1/2} \Delta p_v \tag{S2}$$

$$N_l = \frac{\rho d^3 L}{12\eta\delta_l}\Delta p_l \tag{S3}$$

eqn (S2) can be further modified as:

$$N_v = \frac{3\beta}{8} dL\left(\frac{32M}{9\pi RT}\right)^{1/2} \Delta p_v \tag{S4}$$

β is determined by eqn (S5):

$$\beta = 1 + y^2 - y\sqrt{y^2+1} - \frac{[(2-y^2)\sqrt{y^2+1} + y^3 - 2]^2}{4.5y\sqrt{y^2+1} - 4.5ln(y+\sqrt{y^2+1})} \tag{S5}$$

y is determined by eqn (S6):

$$y = \frac{\delta_v}{2d} \tag{S6}$$

In eqn (S3), Δp_l is the driving force of liquid phase:

$$\Delta p_l = p_f - p_s \tag{S7}$$

However, the liquid-vapor interface inside the 2D nanochannels would further introduce Laplace pressure as driving force into the pervaporation mass transfer process. Therefore, eqn (S7) could be rewritten as:

$$\Delta p_l = p_f - p_s + p_c \tag{S8}$$

In eqn (S8), p_c (Pa) is the Laplace pressure, calculated by surface tension at the interface (σ, N m^{-1}) and contact angle (θ, ^{o}):

$$p_c = \frac{2\sigma cos\theta}{d} \tag{S9}$$

The mass transfer model was established based on eqn (S2)-(S9). Thus, the heat transfer model was further modified as after integration:

$$T(x) = \frac{-N_v \Delta H_v}{dLk_l} \exp\left(\frac{-u\delta_l}{\alpha}\right) \frac{\alpha}{u} \exp\left(\frac{ux}{\alpha}\right) + T_f + \frac{N_v \Delta H_v}{dLk_l} \frac{\alpha}{u} \exp\left(\frac{-u\delta_l}{\alpha}\right) \tag{S10}$$

Considering steady state condition, eqn (S10) was rearranged to:

$$T_s = T_f + \frac{\Delta H_v}{c_p}\left(\exp\left(\frac{-\rho d^2 \Delta p_l c_p}{12\eta k_l}\right) - 1\right) \tag{S11}$$

Therefore, the final model was established. First, a T_s that satisfied eqn (S10) was obtained. Then, δ_l could be obtained from eqn (S3) and (S4). The calculation was conducted in MATLAB R2018b environment.

Fig.S15 Digital photos of tested GO-G_0/PTFE, GO-G_1/PTFE, and GO-G_2/PTFE membranes.

References

1. G. He, M. Xu, J. Zhao, S. Jiang, S. Wang, Z. Li, X. He, T. Huang, M. Cao, H. Wu, M. D. Guiver and Z. Jiang, *Adv. Mater.*, 2017, **29**, 1605898.
2. P. K. Maiti, T. Cagin, G. F. Wang and W. A. Goddard, *Macromolecules*, 2004, **37**, 6236-6254.
3. A. Adson, T. J. Raub, P. S. Burton, C. L. Barsuhn, A. R. Hilgers, K. L. Audus and N. F. H. Ho, *J. Pharm. Sci.*, 1994, **83**, 1529-1536.
4. B. Tansel, J. Sager, T. Rector, J. Garland, R. F. Strayer, L. F. Levine, M. Roberts, M. Hummerick and J. Bauer, *Sep. Purif. Technol.*, 2006, **51**, 40-47.
5. G. H. Li, L. Shi, G. F. Zeng, M. Li, Y. F. Zhang and Y. H. Sun, *Chem. Commun.*, 2015, **51**, 7345-7348.
6. T. A. Peters, C. H. S. Poeth, N. E. Benes, H. Buijs, F. F. Vercauteren and J. T. F. Keurentjes, *J. Membr. Sci.*, 2006, **276**, 42-50.
7. N. Widjojo and T. S. Chung, *Chem. Eng. J.*, 2009, **155**, 736-743.
8. H. Essawy, M. Tawfik, S. El-Sabbagh, A. El-Gendi, E. El-Zanati and H. Abdallah, *Polym. Eng. Sci.*, 2014, **54**, 1560-1570.
9. Y. X. Zhu, S. S. Xia, G. P. Liu and W. Q. Jin, *J. Membr. Sci.*, 2010, **349**, 341-348.
10. T. Liu, Q. F. An, Q. Zhao, K. R. Lee, B. K. Zhu, J. W. Qian and C. J. Gao, *J. Membr. Sci.*, 2013, **429**, 181-189.
11. S. Kalyani, B. Smitha, S. Sridhar and A. Krishnaiah, *Carbohydr. Polym.*, 2006, **64**, 425-432.
12. N. Hu, Y. H. Zheng, Z. Yang, R. F. Zhou and X. S. Chen, *RSC Adv.*, 2015, **5**, 87556-87563.
13. B. X. Huang, Q. Liu, J. Caro and A. S. Huang, *J. Membr. Sci.*, 2014, **455**, 200-206.
14. B. Ben, A. Verhoef, H. M. van Veen, C. Vandecasteele, J. Degreve and B. Van der Bruggen, *Comput. Chem. Eng.*, 2010, **34**, 1775-1788.

15. T. A. Peters, J. Fontalvo, M. A. G. Vorstman, N. E. Benes, R. A. van Dam, Z. Vroon, E. L. J. van Soest-Vercammen and J. T. F. Keurentjes, *J. Membr. Sci.*, 2005, **248**, 73-80.

16. W. Liu, S. Hu, G. Liu, F. Pan, H. Wu, Z. Jiang, B. Wang, Z. Li and X. Cao, *J. Mater. Chem. A.*, 2014, **2**, 5267-5279.

17. D. Hua, R. K. Rai, Y. Zhang and T. S. Chung, *Chem. Eng. Sci.*, 2017, **161**, 341-349.

18. K. Huang, G. P. Liu, J. Shen, Z. Y. Chu, H. L. Zhou, X. H. Gu, W. Q. Jin and N. P. Xu, *Adv. Funct. Mater.*, 2015, **25**, 5809-5815.

19. C. H. Tsou, Q. F. An, S. C. Lo, M. De Guzman, W. S. Hung, C. C. Hu, K. R. Lee and J. Y. Lai, *J. Membr. Sci.*, 2015, **477**, 93-100.

20. Q. Z. Wang, N. Li, B. Bolto, M. Hoang and Z. L. Xie, *Desalination*, 2016, **387**, 46-60.

21. C. H. Cho, K. Y. Oh, S. K. Kim, J. G. Yeo and P. Sharma, *J. Membr. Sci.*, 2011, **371**, 226-238.

22. K. Xu, B. Feng, C. Zhou and A. S. Huang, *Chem. Eng. Sci.*, 2016, **146**, 159-165.

23. B. Liang, W. Zhan, G. G. Qi, S. S. Lin, Q. Nan, Y. X. Liu, B. Cao and K. Pan, *J. Mater. Chem. A*, 2015, **3**, 5140-5147.

24. G. Z. Liu, J. Shen, Q. Liu, G. P. Liu, J. Xiong, J. Yang and W. Q. Jin, *J. Membr. Sci.*, 2018, **548**, 548-558.

25. W. B. Liang, L. Li, J. W. Hou, N. D. Shepherd, T. D. Bennett, D. M. D'Alessandro and V. Chen, *Chem. Sci.*, 2018, **9**, 3508-3516.

26. C. Cheng, L. D. Shen, X. F. Yu, Y. Yang and X. F. Wang, *J. Mater. Chem. A.*, 2017, **5**, 3558-3568.

27. A. S. Huang and B. Feng, *J. Membr. Sci.*, 2018, **548**, 59-65.

28. B. Feng, K. Xu and A. S. Huang, *RSC Adv.*, 2017, **7**, 2211-2217.

29. E. Huth, S. Muthu, L. Ruff and J. A. Brant, *J. Water Reuse Desalin.*, 2014, **4**, 109-124.

30. M. Naim, M. Elewa, A. El-Shafei and A. Moneer, *Water Sci. Technol.*, 2015, **72**, 785-793.

31. B. Liang, K. Pan, L. Li, E. P. Giannelis and B. Cao, *Desalination*, 2014, **347**, 199-206.

32. B. Liang, Q. Li, B. Cao and P. Li, *Desalination*, 2018, **433**, 132-140.

33. B. Zhu, D. T. Myat, J. W. Shin, Y. H. Na, I. S. Moon, G. Connor, S. Maeda, G. Morris, S. Gray and M. Duke, *J. Membr. Sci.*, 2015, **475**, 167-174.

34. Q. Z. Wang, Y. Y. Lu and N. Li, *Desalination*, 2016, **390**, 33-46.

35. S. G. Chaudhri, B. H. Rajai and P. S. Singh, *Desalination*, 2015, **367**, 272-284.

36. M. Drobek, C. Yacou, J. Motuzas, A. Julbe, L. P. Ding and J. C. D. da Costa, *J. Membr. Sci.*, 2012, **415**, 816-823.

37. Z. L. Xie, D. Ng, M. Hoang, T. Duong and S. Gray, *Desalination*, 2011, **273**, 220-225.

38. W. An, X. Zhou, X. Liu, P. W. Chai, T. Kuznicki and S. M. Kuznicki, *J. Membr. Sci.*, 2014, **470**, 431-438.

39. X. W. Qian, N. Li, Q. Z. Wang and S. C. Ji, *Desalination*, 2018, **438**, 83-96.

40. R. Zhang, B. Liang, T. Qu, B. Cao and P. Li, *Environmental technology*, 2017, DOI: 10.1080/09593330.2017.1388852, 1-9.

41. Z. L. Xie, M. Hoang, T. Duong, D. Ng, B. Dao and S. Gray, *J. Membr. Sci.*, 2011, **383**, 96-103.

42. S. G. Chaudhri, J. C. Chaudhari and P. S. Singh, *J. Appl. Polym. Sci.*, 2018, **135**, 13.

43. H. Chamani, T. Matsuura, D. Rana and C. Q. Lan, *J. Membr. Sci.*, 2019, **572**, 332-342.

44. R. R. Nair, H. A. Wu, P. N. Jayaram, I. V. Grigorieva and A. K. Geim, *Science*, 2012, **335**, 442-444.